---

**Article:**
Gadelovits, S.Y., Insepov, D., Kadirkamanathan, V. et al. (2 more authors) (2019) UDE-based controller equipped with a multiple-time-delayed filter to improve the voltage quality of inverters. IEEE Transactions on Industrial Electronics, 66 (11). pp. 8947-8957. ISSN 0278-0046

https://doi.org/10.1109/tie.2019.2902825

---

# UDE-Based Controller Equipped with a Multiple-Time-Delayed Filter to Improve the Voltage Quality of Inverters

S.Y. Gadelovits, *Student Member, IEEE*, D. Insepov, V. Kadirkamanathan, Q.-C. Zhong, *Fellow, IEEE*, and A. Kuperman, *Senior Member, IEEE*

***Abstract*—In this paper, a two-degrees-of-freedom control algorithm based on uncertainty and disturbance estimator (UDE), aimed to minimize the total harmonic distortion of inverter output voltage is proposed, possessing enhanced robustness to fundamental frequency variations. A multiple-time-delay action is combined with a commonly utilized low-pass UDE filter to increase the range of output impedance magnitude minimization around odd multiples of fundamental frequency for enhanced rejection of typical single-phase nonlinear loads harmonics. Marginal robustness improvement achieved by increasing the number of time delays is quantified analytically and revealed to be independent of delay order. The performance of the proposed control approach and its superiority over two recently proposed methods is validated successfully by experimental results.**

***Index Terms*—Uncertainty and disturbance estimator, time-delayed filter, inverter, voltage quality, two degrees of freedom control.**

## I. Introduction

POWER inverters are a key element associated with DC-AC energy conversion applications [1]. Therefore, the research related to the field of inverters control is on-going and extremely popular. Minimizing the total harmonic distortion (THD) of DC-AC power converters feeding nonlinear loads is one of the fundamental challenges [2] – [5]. The challenge of THD reduction is equivalent to inverter output impedance minimization and is therefore closely related to the algorithm utilized for output voltage control [6]. In fact, reducing the magnitude of inverter output impedance around frequencies associated with load energy improves the output voltage quality [7]. In case single-phase inverter feeds a nonlinear load, inverter output impedance magnitude at odd harmonic frequencies is relevant for THD minimization, while in case of three-phase conversion, $6n\pm1$ harmonic components are of interest. In [8] – [11], multi-resonant and repetitive controllers were utilized, to minimize inverter output voltage THD. Despite proven exceptional performance, typical multi-resonant and repetitive control methods possess single-degrees-of-freedom structure, imposing coupling between tracking and disturbance rejection. On the other hand, disturbance observer (DOB) based methods [12], [13] employ two-degrees-of-freedom structures, allowing elimination of the above-mentioned coupling. DOB-based controllers estimate and cancel the lumped uncertainty and disturbance to "nominalize" the plant [14], letting the tracking controller to shape the tracking response of the nominal system.

Uncertainty and Disturbance Estimator (UDE), developed in [15] – [17] and verified to be capable of successfully coping with a variety of control tasks in [18] – [21], is a subset of DOB. It was demonstrated in [22], that UDE-based controllers in may impose disturbance rejection by direct shaping of output impedance via suitable filter design. There, UDE controller equipped with a multi-band-stop-filter (MBS) was utilized to tackle the challenge of inverter output voltage quality enhancement. In [23], UDE controller equipped with a time-delayed-filter (TD) was proposed to improve its ability to approximate and eliminate signals characterized by periodic behavior and applied in [24] to single-phase inverter output voltage quality enhancement. Performance comparison between systems based on the two filters above under similar operating conditions indicated the superiority of TD in terms of both output voltage THD and settling time and the supremacy of MBS in terms of robustness to fundamental frequency variations. Therefore, this paper mainly aims to improve the performance of UDE based controller equipped with a time-delayed-filter in terms of robustness to fundamental frequency variations by increasing the number of delays in the time-delayed-filter, i.e. utilizing a multiple-time-delayed filter (MTD) rather than single-time-delayed filter, employed in [23] and [24].

It must be emphasized that utilizing a TD-based UDE yielded results somewhat similar to repetitive-like action [25]. Yet, as indicated in [23], the proposed method possesses significant fundamental difference owing to the two-degrees-of-freedom structure. Nevertheless, due to revealed similarities, design rules and underlying constraints of odd-harmonic repetitive control [26] – [28] are very helpful in designing TD-based UDE. Methods to improve the robustness of TD-based UDE to fundamental frequency variations by increasing the he number of delays in the time-delayed-filter were proposed in [29] – [31], elaborated in [32] and applied to control of power converters (still utilizing single-degree-of-freedom structure) in [33], [34]. Here, similar enhancement is adopted to equip the UDE with MTD while maintaining the two-degrees-of-freedom structure to improve the robustness to fundamental frequency variations

The rest of the paper is organized as follows. The proposed UDE-based controller is revealed in detail in Section II. Application to improving output voltage quality of inverters is described in Section III. Experimental verification of the proposed methodology is demonstrated in Section IV. The paper is concluded in Section V.

This article has been accepted for publication in a future issue of this journal, but has not been fully edited. Content may change prior to final publication. Citation information: DOI 10.1109/TIE.2019.2902825, IEEE Transactions on Industrial Electronics



## II. UDE-BASED CONTROLLER

Consider a stable, minimum-phase uncertain plant $P$ with disturbance,

$$y(s) = P(s)u(s) = \underbrace{(P_n(s) + \Delta P(s))}_{P(s)}\underbrace{\left(u_c(s) + f(s)\right)}_{u(s)}, \quad (1)$$

where $y$ is the system output, $P_n$ and $\Delta P$ are nominal and uncertain parts of $P$, respectively, $u$ is the plant input, $u_c$ is the control input and $f(t)$ is the external disturbance, satisfying

$$f(t) = \sum_{n=1,odd}^{\infty} F_n \sin(n\omega_0 t + \phi_n), \quad (2)$$

where $F_n$ is the amplitude and $\phi_n$ is the phase of the n$^{th}$ disturbance input harmonic. Reference signal to be tracked by the system output $y(t)$ is given by

$$y^*(t) = R\sin\omega_0 t. \quad (3)$$

Rearranging (1) yields

$$y(s) = P_n(s)\left(u_c(s) + u_d(s)\right) \quad (4)$$

with

$$u_d(s) = f(s) + P_n^{-1}(s)\Delta P(s)u(s) \quad (5)$$

symbolizing the lumped uncertainty and disturbance (LUD), which may be expressed (cf. (1)-(4)) as

$$u_d(t) = \sum_{n=1,odd}^{\infty} D_n \sin(n\omega_0 t + \theta_n), \quad (6)$$

where $D_n$ is the amplitude and $\theta_n$ is the phase of n$^{th}$ disturbance harmonic. Tracking and disturbance rejection requirements are proposed to be met simultaneously by employing a two-degree-of-freedom control structure with a split control signal

$$u_c(t) = u_{ct}(t) - u_{cd}(t) \quad (7)$$

with $u_{ct}(t)$ and $u_{cd}(t)$ symbolizing the output of tracking controller and LUD estimator, respectively. In case the LUD estimator is properly designed, then $u_{cd}(t) \approx u_d(t)$ and (4) reduces to

$$y(s) = P_n(s)u_{ct}(s), \quad (8)$$

i.e. the plant is nominalized [14] and the tracking controller may be designed according to nominal desired behavior. It was shown in [35], [36] that tracking controller and LUD estimator designs may be decoupled under the restriction of available control bandwidth and desired stability margins.

### A. LUD estimator equipped with multiple-time-delayed filter

According to (4), the LUD is given by

$$u_d(s) = P_n^{-1}(s)y(s) - u_c(s). \quad (9)$$

UDE-based controllers reconstruct the LUD in (6) by passing (9) through a linear filter $G_f(s)$, ideally characterized by unity gain and zero phase at odd multiples of $\omega_0$,

$$u_{cd}(s) = u_d(s)G_f(s) = \left(P_n^{-1}(s)y(s) - \underbrace{(u_{ct}(s) - u_{cd}(s))}_{u_c(s)}\right)G_f(s). \quad (10)$$

Rearranging, the LUD estimate is given by

$$u_{cd}(s) = \frac{G_f(s)}{1 - G_f(s)}\left(P_n^{-1}(s)y(s) - u_{ct}(s)\right), \quad (11)$$

making use of system output, tracking control input and nominal plant model only. Moreover, substituting (10) into (4) gives

$$y(s) = P_n(s)\{u_t(s) + u_d(s)\underbrace{(1 - G_f(s))}_{H_f(s)}\}. \quad (12)$$

Apparently, if $G_f(s)$ possesses unity gain and zero phase at odd multiples of $\omega_0$, then corresponding $H_f(s) = 0$ and LUD in (6) will is fully attenuated. Since the LUD in (6) contain odd harmonics only, then

$$u_d(t) = -u_d\left(t - \frac{T_0}{2}\right) \quad (13)$$

with $T_0 = \frac{2\pi}{\omega_0}$, or [36]

$$u_d(s) = -u_d(s)e^{-\frac{T_0}{2}s}. \quad (14)$$

Unfortunately, (13) cannot be utilized as is due to infinite bandwidth. Therefore, (14) is combined with a low-pass filter $Q(s)$ to limit the signal bandwidth, yielding the LUD estimate given by

$$u_{cd}(s) = u_d(s)\left(\underbrace{-Q(s)e^{-\left(\frac{T_0}{2} - \Delta T\right)s}}_{G_{f1}(s)}\right) \quad (15)$$

with $\Delta T$ denoting the delay of $Q(s)$ at $\omega_0$ [23]. The resulting $G_{f1}(s)$ is referred to as time-delayed filter in [24]. Within the pass band of $Q(s)$,

$$H_{f1}(s) \overset{\Delta}{=} 1 - G_{f1}(s) = 1 + e^{-\frac{T_0}{2}s} \quad (16)$$

with corresponding magnitude given by

$$\left|H_{f1}(j\omega)\right| = \left(2 + 2\cos\left(\frac{T_0}{2}\omega\right)\right)^{\frac{1}{2}}. \quad (17)$$

Therefore,

$$\left|H_{f1}(jn\omega_0)\right| = \begin{cases} 0, & odd\ n \\ 2, & even\ n \end{cases} \quad (18)$$

and

$$\left|H_{f1}(j\omega)\right| \le 1 \text{ for } n - \frac{1}{3} \le \frac{\omega}{\omega_0} \le n + \frac{1}{3},\ n\ odd. \quad (19)$$

Bode diagram of $|H_{f1}(j\omega)|$ versus normalized frequency $\omega/\omega_0$ is depicted in Fig. 1. Obviously, the value of $|H_{f1}(j\omega)|$ is close to zero at odd multiplies of the fundamental frequency. On the other hand, it is close to 2 at even multiplies of the fundamental frequency, demonstrating the well-known "waterbed effect".

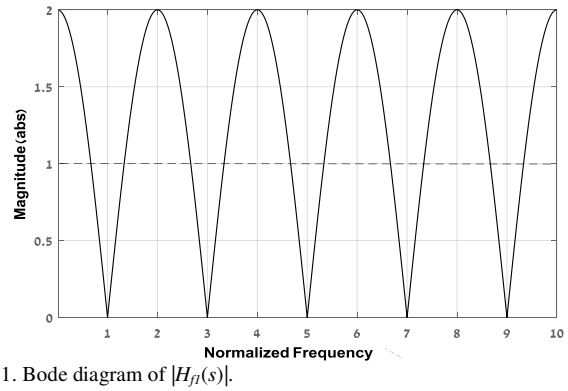


Fig. 1. Bode diagram of $|H_{f1}(s)|$.

In order to improve the LUD estimator robustness to

This article has been accepted for publication in a future issue of this journal, but has not been fully edited. Content may change prior to final publication. Citation information: DOI 10.1109/TIE.2019.2902825, IEEE Transactions on Industrial Electronics



frequency variations, note that (13) may be generalized as

$$u_d(t) = (-1)^m u_d(t - m T_0/2),\ m = 1,2,3... \tag{20}$$

or

$$u_d(s) = (-1)^m u_d(s) e^{-m\frac{T_0}{2}s}. \tag{21}$$

Furthermore, (21) can be rewritten as

$$u_d(s) = \sum_{m=1}^{M} k_m (-1)^m u_d(s) e^{-m\frac{T_0}{2}s} \tag{22}$$

with

$$\sum_{m=1}^{M} k_m = 1. \tag{23}$$

Again, (22) cannot be utilized as is due to infinite bandwidth. Combining with a low-pass filter $Q(s)$ yields the LUD estimate given by

$$u_{cd}(s) = u_d(s) \underbrace{\left( Q(s) \sum_{m=1}^{M} k_m (-1)^m e^{-\left(m\frac{T_0}{2} - \Delta T\right)s} \right)}_{G_{fM}(s)}. \tag{24}$$

The resulting $G_{fM}(s)$ is thereafter referred to as multiple-time-delayed filter. Coefficients $k_m$ are selected following [30], [31] to reduce the sensitivity of $G_{fM}(s)$ to frequency variations around odd multiples of $\omega_0$ by forcing

$$\left. \frac{d^l G_{fM}(s)}{ds^l} \right|_{s = jn\omega_0, n\ odd} = 0,\ l = 1,2,..,M-1, \tag{25}$$

yielding the following system of $M-1$ equations,

$$\sum_{m=1}^{M} m^l k_m = 0,\ l = 1,2,..,M-1. \tag{26}$$

Combining (26) with (23), the solution is given in a matrix form by

$$\mathbf{K} = \mathbf{A}^{-1}\mathbf{B}, \tag{27}$$

where $\mathbf{K} = (k_1, k_2, \ldots, k_M)^T$ is a $M$x1 vector, $\mathbf{A} = \{a_{ij}\}$ is a $M$x$M$ matrix with $a_{ij} = j^{i-1}$ and $\mathbf{B} = (1,0,\ldots,0)^T$ is a $M$x1 vector. Values of $k_m$ for $l = 2$, 3, 4 and 5 are summarized in Table I. Within the pass band of $Q(s)$ (i.e. for $Q(s) = 1$),

$$H_{fM}(s) = 1 - G_{fM}(s) = 1 - \sum_{m=1}^{M} k_m (-1)^m e^{-m\frac{T_0}{2}s} \tag{28}$$

with corresponding magnitude given by

$$\left| H_f(j\omega) \right| = \left( 2 + 2\cos\left( \frac{T_0}{2}\omega \right) \right)^{\frac{1}{2}M}. \tag{29}$$

TABLE I
WEIGHTING COEFFICIENTS OF MULTIPLE-TIME-DELAYED FILTERS

| $M$ | $k_1$ | $k_2$ | $k_3$ | $k_4$ | $k_5$ |
|---|---|---|---|---|---|
| 1 | 1 | -- | -- | -- | -- |
| 2 | 2 | -1 | -- | -- | -- |
| 3 | 3 | -3 | 1 | -- | -- |
| 4 | 4 | -6 | 4 | -1 | -- |
| 5 | 5 | -10 | 10 | -5 | 1 |

Therefore,

$$\left| H_{fM}(jn\omega_0) \right| = \begin{cases} 0, & odd\ n \\ 2^M, & even\ n \end{cases} \tag{30}$$

and

$$\left| H_{fM}(j\omega) \right| \le 1 \text{ for } n - \frac{1}{3} \le \frac{\omega}{\omega_0} \le n + \frac{1}{3},\ n\ odd, \tag{31}$$

i.e. (31) is independent of $M$. Bode diagram of $|H_{fM}(j\omega)|$ versus normalized frequency $\omega/\omega_0$ is depicted in Fig. 2 for $M$ = 1…4. It may be concluded that increasing the number of delays from $M$ to $M + 1$ leads to robustness improvement of $R_{H1}(j\omega) =$

$$\frac{\left| H_{fM}(j\omega) \right|}{\left| H_{fM+1}(j\omega) \right|} = \left| H_{f1}(j\omega) \right|^{-1} = \left( 2 + 2\cos\left( \frac{T_0}{2}\omega \right) \right)^{-\frac{1}{2}} \tag{32}$$

within frequency range given in (31) irrespectively of $M$, as shown in Fig. 3. It may be concluded that the robustness improvement is significant for small frequency deviations around $n$ and reduces to unity (no improvement) towards $n \pm \frac{1}{3}$. Since in practical cases expected frequency deviations are quite small, substantial robustness improvement may be expected.

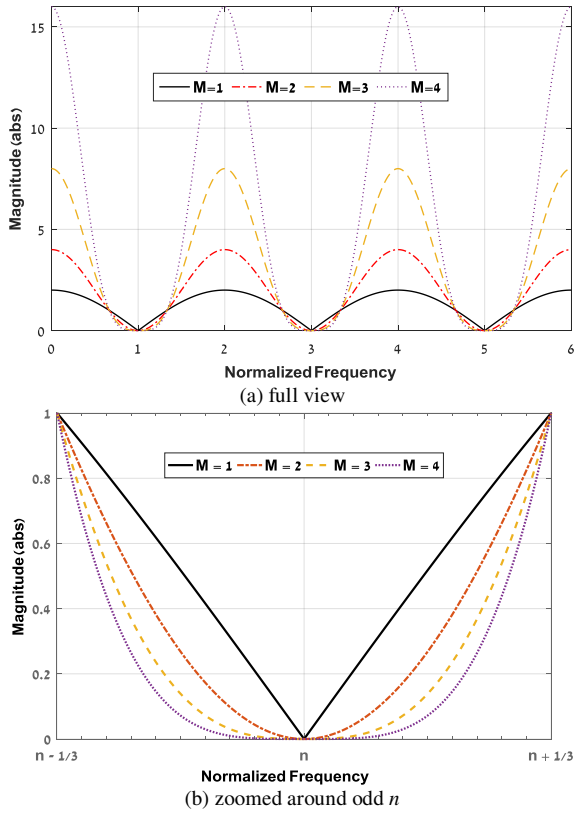


(a) full view

(b) zoomed around odd $n$

Fig. 2. Bode diagram of $|H_{fM}(s)|$ with $Q(s) = 1$ for different values of $M$.

Application of a non-ideal low-pass filter $Q(s)$ with cut-off frequency $\omega_F$ influences $H_{fM}(s)$ as follows: for $\omega << \omega_F$, (29) – (32) remain valid while for $\omega \to \omega_F$ performance degradation takes place, as pointed out in [23]. Bode diagram of $|H_{fM}(j\omega)|$ combined with a $\omega_F = 20\omega_0$ first-order Butterworth filter versus normalized frequency is depicted in Fig. 4 for $M$ = 1, 2, 3, 4 to demonstrate the effect of non-ideal $Q(s)$ application. Consequently, bandwidth of $Q(s)$ should be as high as possible to preserve idealized behavior given by (29) – (32) for as many harmonics as possible.

This article has been accepted for publication in a future issue of this journal, but has not been fully edited. Content may change prior to final publication. Citation information: DOI 10.1109/TIE.2019.2902825, IEEE Transactions on Industrial Electronics



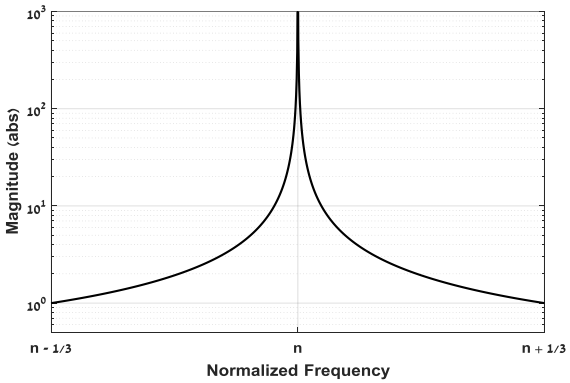


Fig. 3. Bode diagram of $|R_{H1}(s)|$ zoomed around odd $n$.

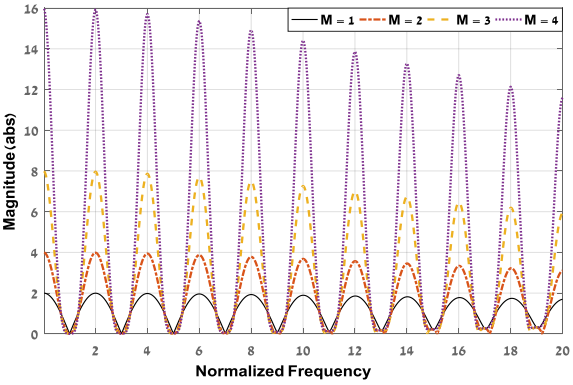


(a) full view

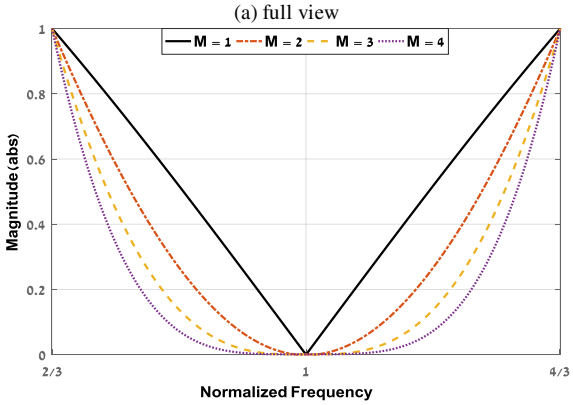


(b) zoomed around $n = 1$

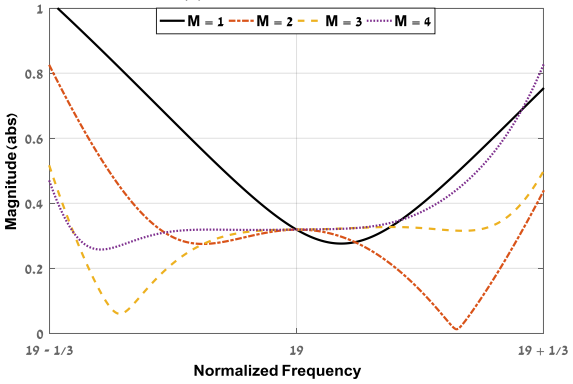


(c) zoomed around $n = 19$

Fig. 4. Bode diagram of $|H_{fM}(s)|$ with low-pass $Q(s)$ for different values of $M$.

## B. Tracking controller

Once (8) is valid, the plant is LUD-free and tracking controller $C_t(s)$ may be selected according to desired nominal tracking performance. In general, to assure zero steady-state tracking error, a proportional-resonant controller should be selected for a reference given by (3) [38]. Nevertheless, in case the nominal plant is a pure integrator (typical for power electronic converters under cascaded current-voltage control), proportional controller may be sufficient in case available control bandwidth is much higher (decade or more) than $\omega_0$. The output of tracking controller $C_t(s)$ is given by

$$u_{ct}(s) = C_t(s)\left(y^*(s) - y(s)\right). \tag{34}$$

## C. Combined control action

Following (7), the control signal $u_c(t)$ is formed by the difference between (34) and (24) as

$$u_c(s) = C_t(s)\left(y^*(s) - y(s)\right) - \\ -\frac{G_{fM}(s)}{1-G_{fM}(s)}\left(P_n^{-1}(s)y(s) - C_t(s)\left(y^*(s) - y(s)\right)\right). \tag{35}$$

Rearranging, there is

$$u_c(s) = \frac{C_t(s)}{1-G_{fM}(s)}y^*(s) - \frac{C_t(s)+G_{fM}(s)P_n^{-1}(s)}{1-G_{fM}(s)}y(s). \tag{36}$$

In case a limited bandwidth actuator $T_a(s)$ is present, plant input and output are given by

$$u(s) = u_c(s)T_a(s) + u_d(s) \tag{37}$$

and

$$y(s) = \frac{P_n(s)C_t(s)}{1+P_n(s)C_t(s)}y^*(s) + \frac{\left(1-G_{fM}(s)\right)P_n(s)}{\left(1+P_n(s)C_t(s)\right)T_a(s)}u_d(s), \tag{38}$$

respectively. Apparently, in case the energy content of $u_d(s)$ is concentrated at multiples of $\omega_0$, system output would satisfy the desired tracking behavior in steady state. Overall control block diagram is depicted in Fig. 5.

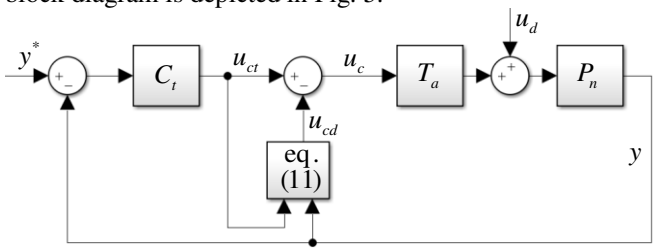


Fig. 5. Overall block diagram of the proposed control structure.

Nominal system loop gain is derived as

$$L_n(s) = \frac{P_n(s)C_t(s)+G_{fM}(s)}{1-G_{fM}(s)}T_a(s) \\ = \frac{P_n(s)C_t(s)+Q(s)\sum_{m=1}^{M}k_m(-1)^m e^{-\left(m\frac{T_0}{2}-\Delta T\right)s}}{1-Q(s)\sum_{m=1}^{M}k_m(-1)^m e^{-\left(m\frac{T_0}{2}-\Delta T\right)s}}T_a(s). \tag{39}$$

As recently shown in [35], [36], trade-off between tracking and disturbance rejection would always appear due to finite available control bandwidth and must be accordingly accounted upon selection of the tracking controller $C_t(s)$, delay order $M$ and the filter $Q(s)$.

This article has been accepted for publication in a future issue of this journal, but has not been fully edited. Content may change prior to final publication. Citation information: DOI 10.1109/TIE.2019.2902825, IEEE Transactions on Industrial Electronics



## III. APPLICATION TO IMPROVING THE VOLTAGE QUALITY OF INVERTERS

A single-phase inverter with LC filter, fed from a dc source $v_{DC}$ is shown in Fig. 6. Inverter leg voltage, inductor current and output voltage are denoted as $u_0$, $i_L$ and $v_O$, respectively. PWM signal, modulated by the control input $v$ drives the converter leg. Practical nonlinear loads, connected to inverter output terminals, draw currents $i_O(t)$ satisfying (2). On the other hand, output voltage reference is of the form (3). A cascaded dual-loop control structure is utilized (similarly to [22], [24]). Inductor current dynamics is given by

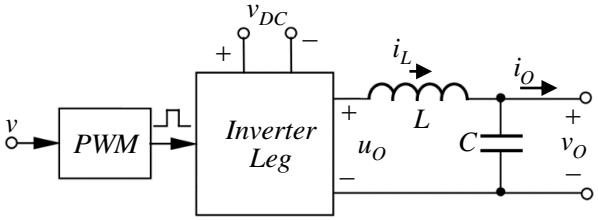


Fig. 6. Single-phase LC-filter based inverter.

$$\frac{di_L(t)}{dt} = L^{-1}\left(v(t-T_d)v_{DC}(t) - v_O(t)\right), \tag{40}$$

with $T_d$ symbolizing the total sampling and switching delay. The control input is selected as

$$v(t) = \frac{1}{v_{DC}(t)}\left(K_{PI}\left(i_L^*(t) - i_L(t)\right) + v_O(t)\right), \tag{41}$$

where $i_L^*(t)$ is inductor current reference signal and $K_{PI}$ is proportional gain. Complementary sensitivity function is then obtained as

$$T_I(s) = \frac{i_L(s)}{i_L^*(s)} = \frac{K_{PI}L^{-1}}{se^{T_d s} + K_{PI}L^{-1}}. \tag{42}$$

which serves as the voltage loop actuator and is equivalent to $T_a$ introduced in (37).

Consider an inverter of Fig. 6 with numerical values of relevant parameters summarized in Table II. Setting $K_{PI}$ to 59 combined with double update modulation, yields a 2762 Hz bandwidth current loop with 45° phase margin and 6dB gain margin as in [22]. Note that $T_d$ is a combination of half cycle delay and the computational time delay and equals to $45\mu s$. Bode diagram of the resulting current loop complementary sensitivity function $T_I(s)$ is given in Fig. 7.

TABLE II
NOMINAL SYSTEM PARAMETER VALUES

| Parameter | Value | Units |
|---|---|---|
| Switching frequency, $T_S^{-1}$ | 15 | *kHz* |
| Sampling Frequency | 30 | *kHz* |
| Filter inductance, $L$ | 3.4 | *mH* |
| Filter capacitance, $C_n$ | 30 | $\mu F$ |
| Fundamental frequency, $\omega_0$ | 100π | *rad/s* |
| DC link voltage, $v_{DC}$ | 195 | *V* |
| Reference magnitude, $V_1$ | 110√2 | *V* |

Output voltage dynamics may then be expressed by (cf. (4) and (37))

$$v_O(s) = \underbrace{\frac{1}{C_n s}}_{P_n(s)}\Big(\underbrace{i_L^*(s)}_{u_c(s)}\underbrace{T_I(s)}_{T_a(s)} + \underbrace{i_d(s)}_{u_d(s)}\Big) \tag{43}$$

with $C = C_n + \Delta C$ and

$$i_d(s) = -i_O(s) + C_n^{-1}\Delta C_n^{-1}\left(i_L^*(s)T_I(s) + i_O(s)\right). \tag{44}$$

From (2), (3) and (38), output voltage is given by

$$v_O(t) = \sum_{n=1,\ odd}^{\infty} V_n \sin(n\omega_0 t + \psi_n), \tag{45}$$

i.e. in order to track the reference (3) with $R = V_1$, then $\psi_1$ and $V_n$ (for $n > 1$) should be minimized. In other words, inverter output voltage should be in phase with the reference (tracking controller goal) and harmonic distortion free (disturbance observer goal). Total harmonic distortion of the output voltage is defined by

$$THD_V = \sqrt{\sum_{n=3,odd}^{\infty}\left(\frac{V_n}{V_1}\right)^2} = V_1^{-1}\sqrt{\sum_{n=3,odd}^{\infty}\left(I_{dn}\left|Z_O(jn\omega_0)\right|\right)^2}, \tag{46}$$

where $I_{dn}$ is the $n$-th harmonic magnitude of $i_d(t)$ (cf. (44)).

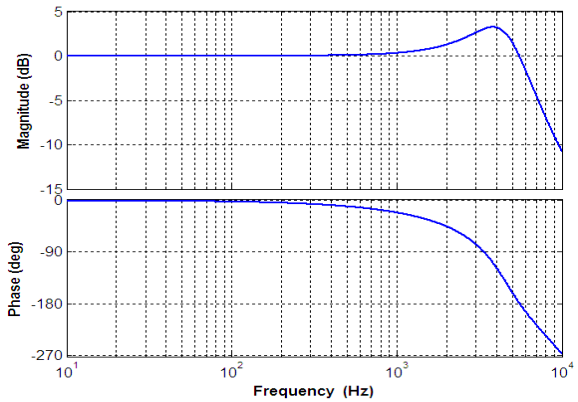


Fig. 7. Bode diagram of voltage loop actuator $T_I(s)$.

From (38), the inverter output voltage is (cf. (38))

$$v_O(s) = \underbrace{\frac{P_n(s)C_t(s)}{1+P_n(s)C_t(s)}}_{T_v(s)}v^*(s) + \underbrace{\frac{\left(1-G_{fM}(s)\right)P_n(s)}{\left(1+P_n(s)C_t(s)\right)T_a(s)}}_{Z_o(s)}i_d(s), \tag{47}$$

where $T_v$ is the voltage tracking transfer function and $Z_o$ is the inverter output impedance. Obviously, since $H_{fM}(s)$ is designed according to (28), then $|Z_O(jn\omega_0)| \to 0$, i.e. low (ideally zero) THD may be expected.

The control input in (43) is split as (cf. (7))

$$\underset{u_c(s)}{i_L^*(s)} = \underset{u_{ct}(s)}{i_{Lt}^*(s)} - \underset{u_{cd}(s)}{i_{Ld}^*(s)}, \tag{48}$$

where the first term on the right-hand side denotes the tracking controller output given by

$$i_{Lt}^*(s) = K_{PV}\left(v_O^*(s) - v_O(s)\right) \tag{49}$$

with proportional gain $K_{PV}$ and the second one symbolizes the disturbance observer output, given by

$$i_{Ld}^*(s) = \frac{G_{fM}(s)}{1-G_{fM}(s)}\left(C_n s v_O(s) - u_{ct}(s)\right). \tag{50}$$

The filter $G_{fM}(s)$ was defined in (24) with $Q(s)$ selected as a third-order Butterworth filter (see the discussion on filter order selection in [23])

$$Q(s) = \frac{\omega_F^3}{s^3 + 2\omega_F s^2 + 2\omega_F^2 s + \omega_F^3}, \tag{51}$$

yielding

$$\Delta T = \frac{1}{\omega_0} tg^{-1}\left(\frac{2\omega_F^2\omega_0 - \omega_0^3}{\omega_F^3 - 2\omega_0^2\omega_F}\right). \tag{52}$$

Since the only voltage plant parameter is the capacitance $C$, whose value is not expected to undergo significant variations, phase margin (PM) of 30° and gain margin (GM) of 5dB are sufficient for stability assurance. If required, larger stability margins may be attained by trading off tracking bandwidth (i.e. $K_{PV}$) or $\omega_F$.

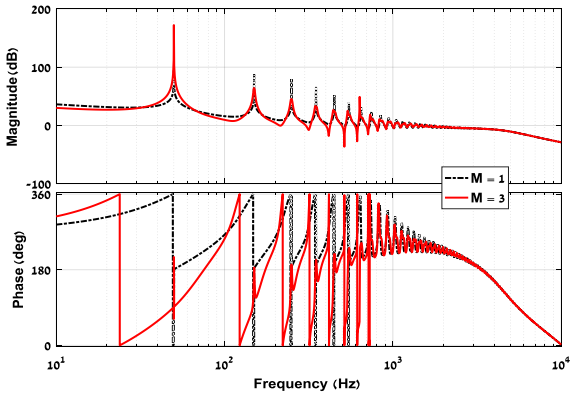


Fig. 8. Bode diagrams of $L_n(s)$ for $M = 1, 3$.

TABLE III
FILTER BANDWIDTHS AND STABILITY MARGINS FOR DIFFERENT NUMBER OF DELAYS

| $M$ | $\omega_F$, rad/s | $PM$, ° | $GM$, $dB$ |
|---|---|---|---|
| 1 | $2\pi \cdot 840$ | 38 | 5 |
| 2 | $2\pi \cdot 640$ | 30 | 5.3 |
| 3 | $2\pi \cdot 590$ | 30 | 5.3 |

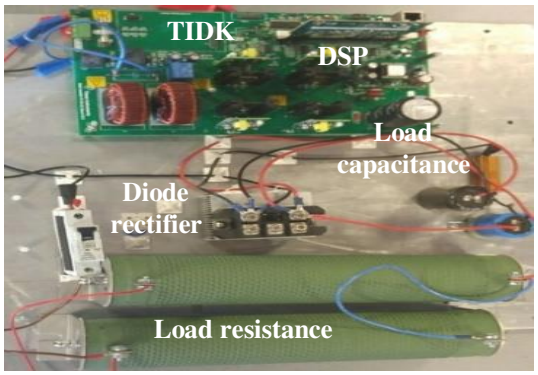


Fig. 9. Experimental setup.

It was shown in [24] that for $M = 1$, increasing the order of $Q(s)$ imposes $\omega_F$ reduction for given stability margin constraints. Here, the filter order remains unchanged and the number of delays $M$ is increased from 1 to 3. For each number of delays, maximum $\omega_F$ is searched for until one of the stability margins limits is reached. The results are summarized in Table III and Bode diagrams of corresponding nominal loop gains $L_n(s)$ (cf. (40)) for $M = 1$, 3 and $K_{PV} = 0.236$ (i.e. tracking loop bandwidth of $2500\pi$ rad/s) are presented in Fig. 8 . As expected, rising the number of delays increases the loop gain robustness) around odd multiples of $\omega_0$ while trading off the peak gain at these frequencies due to decreased $\omega_F$ [23], [39]. In practice, slight peak gain reduction has a negligible influence on performance since the output impedance at relevant harmonics is below the system noise level.

## IV. VERIFICATION

In order to verify the feasibility of the proposed UDE-based filter equipped with a multiple-time-delayed filter, modified Texas Instruments High Voltage Single Phase Inverter Development Kit (TIDK) with parameters in Table I was utilized. The proposed control structure with $M = 3$ and $\omega_F = 2\pi \cdot 590$ rad/s (cf. Table III) was executed in digital form by a Concerto F28M35 control board. Experimental setup is depicted in Fig. 9.

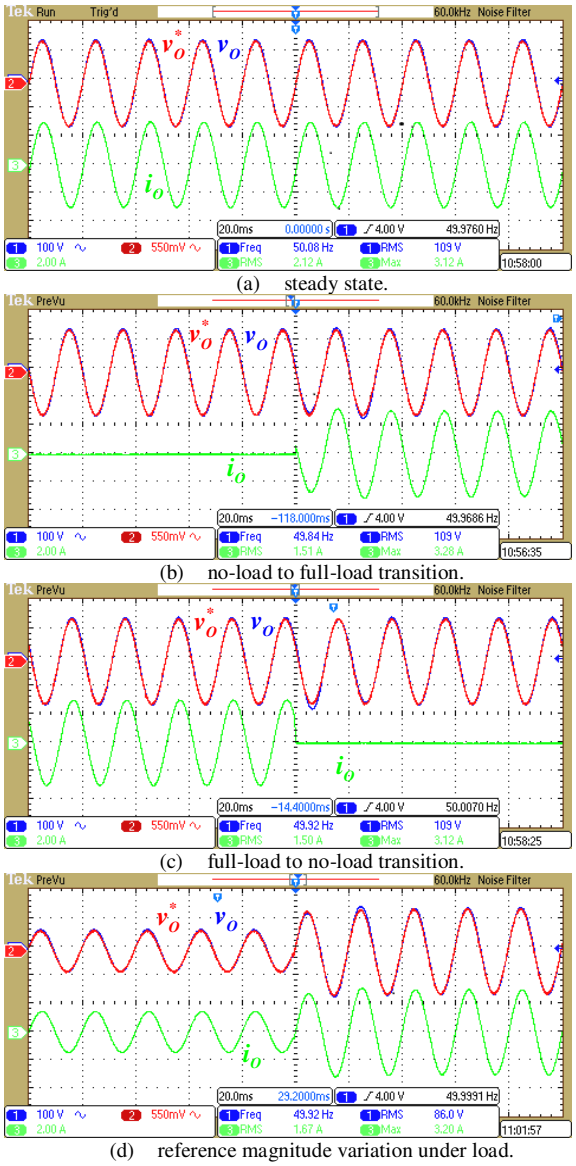


Fig. 10. Experimental results: Operation with linear load.

This article has been accepted for publication in a future issue of this journal, but has not been fully edited. Content may change prior to final publication. Citation information: DOI 10.1109/TIE.2019.2902825, IEEE Transactions on Industrial Electronics



### A. *Operation with linear load*

In order to verify the performance under linear load, a 33Ω resistor was connected across inverter output terminals. Fig. 10(a) presents the steady state operation waveforms, Fig. 10(b) and 10(c) demonstrate full load – to – no load and no load – to – full load transitions, respectively, and Fig. 10(d) shows the response to 50% – to – 100% reference magnitude step change.

Apparently, satisfactory performance is evident in both steady state and transients. Under linear load, the system achieved output voltage THD of 0.88% in steady state operation.

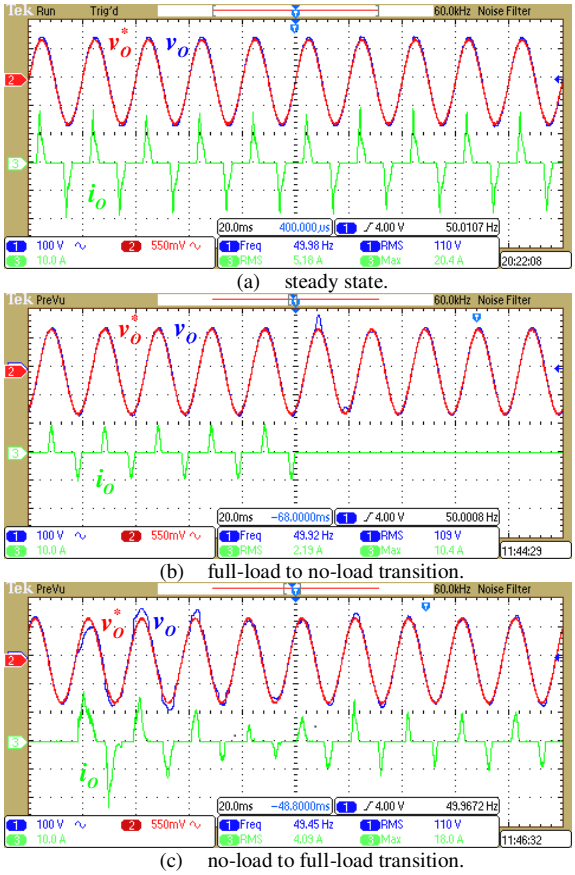


Fig. 11. Experimental results: Steady-state operation with nonlinear load.

### B. *Operation with nonlinear load*

In order to verify the steady-state performance under nonlinear load, the 33Ω resistor was removed and swapped with a full-bridge diode rectifier, terminated by a 50Ω(250W)/940μF parallel RC load with a crest factor of ~3.35. Fig. 11(a) presents respective reference and output waveforms. For transient performance testing, the 50Ω resistor was replaced with a 100Ω one to limit the inrush current. Fig. 11(b) and 11(c) demonstrate full load – to – no load and no load – to – full load transitions, respectively. Under nonlinear load, the system achieved output voltage THD of 1.78% in steady state operation.

### C. *Robustness to fundamental frequency variations*

In order to verify the robustness to fundamental frequency variations, steady-state system operation under nonlinear load was examined for fundamental frequency deviations of ±2Hz. Experimental results are shown in Fig. 12 for the range of ±1Hz (which are likely to occur) and corresponding $THD_V$ values are presented in Fig. 13 for fundamental frequency deviations of ±2Hz. It may be concluded that the system is indeed robust to frequency deviations of ±1Hz. Nevertheless, the $THD_V$ attains its minimum below 50Hz and is asymmetrical. This is well expected from both the fact that $\Delta T$ in (24) accounts for the first harmonic only while the valleys of $|H_f(s)|$ at higher multiples of $\omega_0$ are slightly displaced. Moreover, it is expected from Fig. 4(b) that for $M = 3$, higher load harmonics would be better rejected around harmonic multiples than at their exact position. In order to verify this observation, the filter (24) was re-designed assuming fundamental frequency of 50.25 Hz rather than 50Hz.

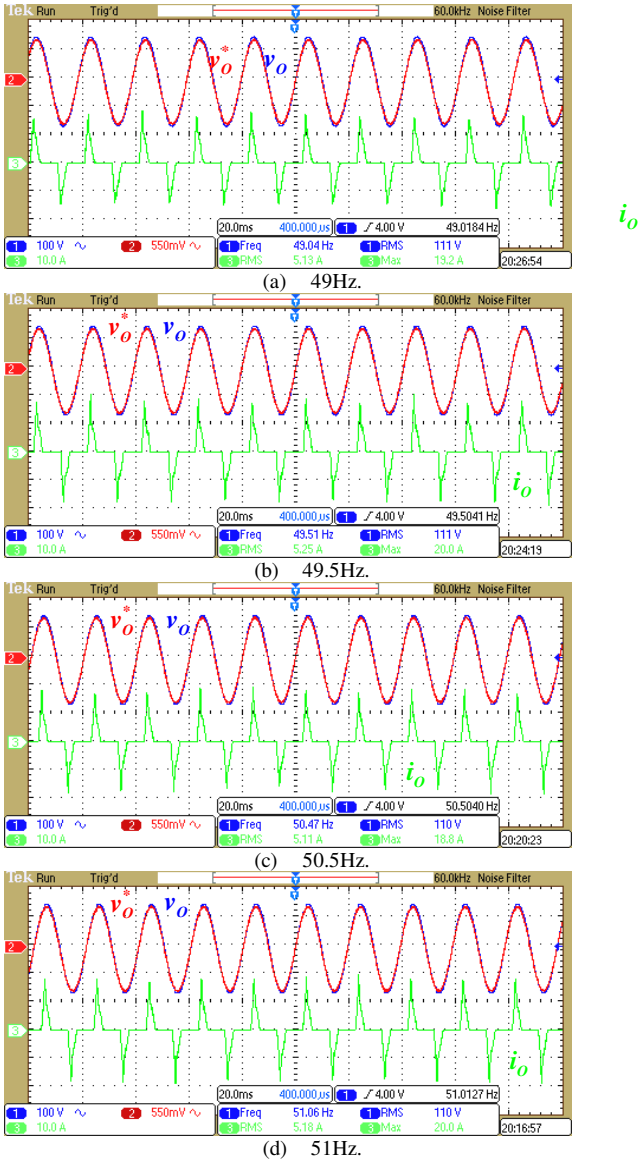


Fig. 12. Experimental results. Steady state operation with nonlinear load under ±1Hz fundamental frequency deviation.

Corresponding $THD_V$ values are presented in Fig. 13 for fundamental frequency deviations of ±2Hz. As the result of

This article has been accepted for publication in a future issue of this journal, but has not been fully edited. Content may change prior to final publication. Citation information: DOI 10.1109/TIE.2019.2902825, IEEE Transactions on Industrial Electronics



re-design, the $THD_V$ curve was shifted to the right with corresponding value at 50Hz reduced from 1.78% to 1.67% and became more symmetrical.

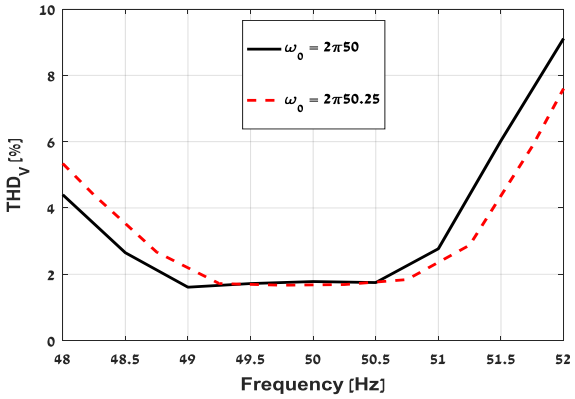


Fig. 13. Experimental results. Robustness to ±2Hz fundamental frequency deviations.

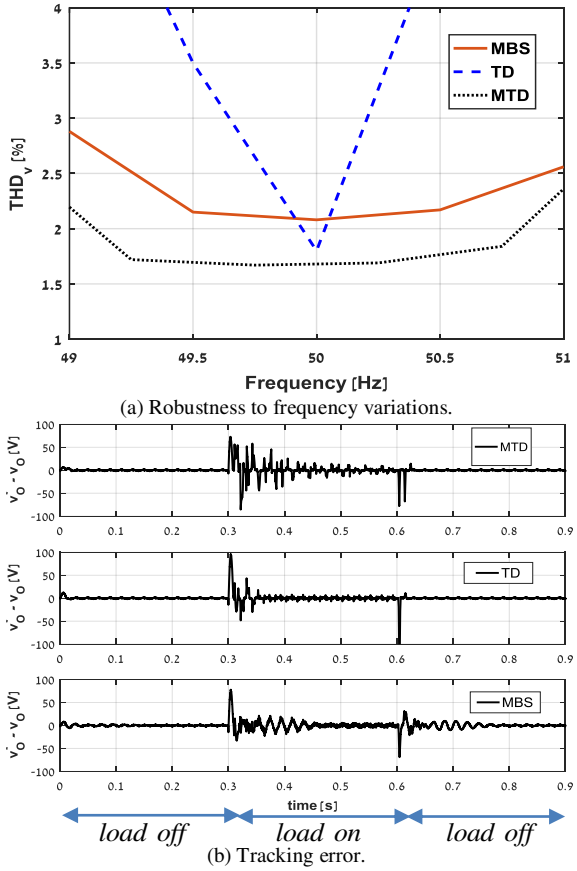


(a) Robustness to frequency variations.

(b) Tracking error.

Fig. 14. Results of comparison with methods proposed in [21] and [23].

### D. *Comparison with multi-band-stop and single-time-delayed filters based UDE*

As mentioned above, in [22] and [24] similar dual-loop control structures were proposed, utilizing different two-degrees-of-freedom regulator as voltage controller. In [22], a UDE equipped with a multi-band-stop filter was utilized for disturbance rejection (equivalent to utilizing a multi-resonant controller) while in [24] a UDE equipped with a single-time-delayed filter was employed. The hardware setup and other operational parameters (switching frequency and load) were similar to the ones in this paper.

Outcomes of performance comparison of control structures in [22] (denoted as MBS), [24] (denoted as TD) and the one proposed here (denoted as MTD) are summarized in Fig. 14. Apparently, MTD is superior both in case the fundamental frequency remains nominal and in case $\omega_0$ is expected to vary, as shown in Fig. 14(a). Fig. 14(b) demonstrates tracking errors of output voltage for no load - to - full load - to - no load transients. In terms of transient response speed, MTD outperforms MBS while being inferior to TD, as expected. This is due to the increased amount of delay utilized, which in turn increases the convergence time of the proposed UDE design. MTD vs MBS experimental output voltage normalized harmonic spectra comparison is depicted in Fig. 15.

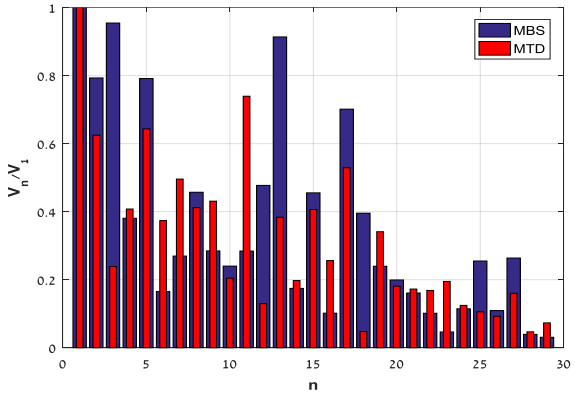


Fig. 15. Normalized harmonic spectra comparison: MTD vs MBS.

## V. Conclusions

In this paper, a two-degrees-of-freedom control structure based on UDE controller equipped with a multiple-time-delayed filter was suggested, aimed to improve the output voltage quality of DC-AC converters by minimizing the inverter output impedance magnitude around odd harmonics of fundamental frequency. Compared to previously proposed UDE controllers equipped with multiple-band-stop and single-time-delay filters, the proposed control structure has yielded lower $THD_V$ for both nominal and varied based frequency. On the other hand, due to the adoption of multiple time delays, the transient response is slightly prolonged compared to the single-time-delayed filter yet still better than that of multiple-band-stop-filter.

## Acknowledgment

Shlomo Y Gadelovits was supported by the Doctoral Prize Scholarship of The Department of Automatic Control and System Engineering, The University of Sheffield.

## References

[1] Q.-C. Zhong and T. Hornik, *Control of Power Inverters in Renewable Energy and Smart Grid Integration*. New York, NY, USA: Wiley-IEEE Press, 2013.

[2] H. Komurcugil, N. Altin, S. Ozdemir and I. Sefa, "Lyapunov-function and proportional-resonant-based control strategy for single-phase grid-connected VSI with LCL filter," *IEEE Trans. Ind. Electron.*, vol. 63, no. 5, pp. 2838-2849, May 2016.

[3] Q.-C. Zhong, "Harmonic droop controller to reduce the voltage harmonics of inverters," *IEEE Trans. Ind. Electron.*, vol. 60, no. 3, pp. 936-945, Mar. 2013.

[4] J. Lim, C. Park, J. Han and Y. Lee, "Robust tracking control of a three-phase DC-AC inverter for UPS applications," *IEEE Trans. Ind. Electron*., vol. 61, no. 8, pp. 4142 – 4151, Aug. 2014.

[5] A. D. Kiadehi, K. El Khamlichi Drissi and C. Pasquier, "Voltage THD reduction for dual-inverter fed open-end load with isolated DC sources," *IEEE Trans. Ind. Electron*., vol. 64, no. 3, pp. 2102 – 2111, Mar. 2017.

[6] J. M. Guerrero, L. G. de Vicuna, J. Matas, M. Castilla, and J. Miret, "Output impedance design of parallel-connected UPS inverters with wireless load-sharing control," *IEEE Trans. Ind. Electron*., vol. 52, no. 4, pp. 1126–1135, May. 2005

[7] Q.-C. Zhong and Y. Zeng, "Control of inverters via a virtual capacitor to achieve capacitive output impedance," *IEEE Trans. Power Electron.*, vol. 29, no. 10, pp. 5568-5578, Oct. 2014.

[8] L. F. A. Pereira, J. V. Flores, G. Bonan, D. F. Coutinho and J. M. G. da Silva Jr., "Multiple resonant controllers for UPS – a systematic robust control design approach," *IEEE Trans. Ind. Electron*., vol. 61, no. 3, pp. 1528 - 1538, Mar. 2014.

[9] A. Lidozzi, M. Di Benedetto, S. Bifaretti, L. Solero and F. Crescimbini, "Resonant controllers with three degrees of freedom for AC power electronics converters," *IEEE Trans. Ind. Appl*., vol. 51, no. 6, pp. 4595 - 4604, Nov./Dec. 2015.

[10] G. Escobar, P. G. Hernandez-Briones, P. R. Martinez, M. Hernandez-Gomez and R. E. Torres-Olguin, "A repetitive-based controller for the compensation of $6l\pm1$ harmonic components," *IEEE Trans. Ind. Electron*., vol. 55, no. 8, pp. 3150–3158, Aug. 2008.

[11] W. Lu, K. Zhou, D. Wang and M. Cheng, "A generic n$k\pm$m-order harmonic repetitive control scheme for PWM converters," *IEEE Trans. Ind. Electron*., vol. 61, no. 3, pp. 1516–1527, Mar. 2014.

[12] W.-H. Chen, K. Ohnishi and L. Guo, "Advances in Disturbance/Uncertainty estimation and attenuation," *IEEE Trans. Ind. Electron*., vol. 62, no. 9, pp. 5758 – 5762, Sep. 2015.

[13] W.-H. Chen, J. Yang, L. Guo and S. Li, "DOB control and related methods – an overview," *IEEE Trans. Ind. Electron*., vol. 63, no. 2, pp. 1083 –1095, Feb. 2016.

[14] A. Kuperman, Y. Horen and S. Tapuchi, "Input-output nominalization of linear plants with slow varying uncertainties," *COMPEL - Int. J. Comp. Math. Electr. Electron. Eng.,* vol. 29, no. 1, pp. 72-89, 2010.

[15] Q.-C. Zhong and D. Rees, "Control of uncertain LTI systems based on UDE," *ASME J. Dyn. Syst. Meas. Control*, vol. 126, pp. 905–910, 2004.

[16] Q.-C. Zhong, A. Kuperman, and R. K. Stobart, "Design of UDE-based controllers from their two-degree-of-freedom nature," *Int. J. Robust Nonl. Control*, vol. 21, no. 17, pp. 1994–2008, 2011.

[17] R. K. Stobart, A. Kuperman and Q.-C. Zhong, "UDE–based control for uncertain LTI-SISO systems with state delays," *ASME J. Dyn. Syst. Meas. Control*, vol. 133, pp. 024502-1-3, 2011.

[18] A. Kuperman and Q.-C. Zhong, "UDE-based linear robust control for a class of nonlinear systems with application to wing rock motion stabilization," *Nonl. Dyn.*, vol. 81, no. 1, pp. 789 – 799, 2015.

[19] B. Ren, Q.-C. Zhong and J. Chen, "Robust control for a class of nonaffine nonlinear systems based on the uncertainty and disturbance estimator," *IEEE Trans. Ind. Electron.*, vol. 62, no. 9, pp. 5881-5888, Sep. 2015.

[20] I. Aharon, D. Shmilovitz and A. Kuperman, "Robust output voltage control of multimode non inverting DC-DC converter," *Int. J. Control*, vol. 90, no. 1, pp. 110–120, Jan. 2017.

[21] Q.-C. Zhong Y.Wang and B. Ren, "UDE-based robust droop control of inverters in parallel operation," *IEEE Trans. Ind. Electron*., DOI: 10.1109/TIE.2017.2677309.

[22] S. Gadelovits, Q.-C. Zhong V. Kadirkamanathan and A. Kuperman, "UDE-based controller equipped with a multi-band-stop filter to improve the voltage quality of inverters," *IEEE Trans. Ind. Electron*., vol. 64, no. 9, pp. 7433 – 7443, Sep. 2017.

[23] N. Alshek, S. Bronshtein, M. Elkayam and A. Kuperman, "Modified uncertainty and disturbance estimator for enhanced periodic signals suppression," *IEEE Trans. Ind. Electron.*, DOI: 10.1109/TIE.2018.2833035.

[24] S. Gadelovits, Q.-C. Zhong V. Kadirkamanathan and A. Kuperman, "UDE-based controller equipped with a time-delayed filter to improve the voltage quality of inverters," *IEEE Trans. Ind. Electron*., DOI: 10.1109/TIE.2018.2831182.

[25] R. Grino and R. Costa-Castello, "Digital repetitive plug-in controller for odd-harmonic periodic references and disturbances," *Automatica*, vol. 41, pp. 153 – 157, 2005.

[26] J. V. Flores, L. F. A. Pereira, G. Bonan, D. F. Coutinho and J. M. G. da Silva Jr., "A systematic approach for robust repetitive controller design," *Contr. Eng. Pract*., vol. 54, pp. 214 – 222, 2016.

[27] K. Zhou, K.-S. Low, D. Wang, F.-L. Luo, B. Zhang and Y. Wang, "Zero-phase odd-harmonic repetitive controller for a single-phase PWM inverter," *IEEE Trans. Power Electron*., vol. 21, no. 1, pp. 193 – 202, Jan. 2006.

[28] G. Escobar, P. R. Martinez, J. Leyva-Ramos and P. Mattavelli, "A negative feedback repetitive control scheme for harmonic compensation," *IEEE Trans. Ind. Electron*., vol. 55, no. 4, pp. 1383 – 1386, Aug. 2006.

[29] T. Singh and s. R. Vadali, "Robust time-delay control," *J. Dyn. Syst. Meas. Contr*., vol. 115, pp. 303 – 306, 1993.

[30] M. Steinbuch, "Repetitive control for system with uncertain period-time," *Automatica*, vol. 38, pp. 2103 – 2109, 2002.

[31] M. Steinbuch, S. Weiland and T. Singh, "Design of noise and period-time robust high-order repetitive control with application to optical storage," *Automatica*, vol. 43, pp. 2086 – 2095, 2007.

[32] G. Pipeleers, B. Demeulenaere, L. De Schutter and J. Swevers, "Robust high-order repetitive control: Optimal performance trade-offs," *Automatica*, vol. 44, pp. 2628 – 2634, 2008.

[33] G. A. Ramos and R. Costa-Castello, "Power factor correction and harmonic compensation using second-order odd-harmonic repetitive control," *IET Contr. Theory Appl*., vol. 6, no. 11, pp. 1633 – 1644, 2012.

[34] G. A. Ramos, R. Costa-Castello and J. M. Olm, "Precompensated second order repetitive control of an active filter under varying network frequency," *Asian J. Contr*., vol. 17, no. 4, pp. 1243 – 1254, Jul. 2015.

[35] I. Aharon, D. Shmilovitz and A. Kuperman, "Uncertainty and disturbance estimator based controllers design under finite control bandwidth constraint," *IEEE Trans. Ind. Electron*., vol. 65, no. 2, pp. 1439 – 1449, Feb. 2018.

[36] I. Aharon, D. Shmilovitz and A. Kuperman, "Phase margin oriented design and analysis of UDE-based controllers under actuator constraints," *IEEE Trans. Ind. Electron.*, DOI: 10.1109/TIE.2018.2801846.

[37] Q.-C. Zhong, Time Delay Control and Its Applications, Ph.D. thesis, Shanghai Jiao Tong University, Shanghai, China, 1999, in Chinese.

[38] A. Kuperman, "Proportional-resonant current controllers design based on desired transient performance," *IEEE Trans. Power Electron*., vol. 30, no. 10, pp. 5341 – 5345, Oct. 2015.

[39] J. S. Freudenberg and D. P. Looze, "Right half plane poles and zeros and design tradeoffs in feedback systems," *IEEE Trans. Aut. Contr*., vol. AC-30, no. 6, pp. 555 – 565, Jun. 1985.

Shlomo Y. Gadelovits received his B.Sc and M.Sc degrees in electrical and electronic engineering from the University of Ariel, Israel, in 2011 and 2013 respectively. From 2011 to 2014 he was with the Hybrid energy sources R&D laboratory. He is currently a Research Associate in the Rolls-Royce supported University Technology Centre in Control and Monitoring Systems Engineering and pursuing his Ph.D. degree in the Department of Automatic Control and Systems Engineering, The University of Sheffield, UK. His research interests include control of power converters, power quality, resonant controllers, and in particular disturbance estimation in AC power control.

Dauren Insepov was born in 1983, Kazakhstan. In 2005, he graduated the M. Tynyshpayev Kazakh Academy of Transport and Communications. In 2011, he received the B. Sc. degree from the Moscow State University of Communications (MIIT). In 2013, he received the M.Sc. degree in electric power engineering from the D. A. Kunayev Humanitarian University of Transport and Law. He is currently pursuing his Ph.D. degree in radio engineering, electronics and telecommunications in the K. I. Satpayev Kazakh National Research Technical University. He was a visiting researcher with the Hybrid Energy Sources Laboratory, Ariel University of Samaria, Israel, in 2016. His research interests include control of power converters and inductive heating,

Visakan Kadirkamanathan obtained his B.A in Electrical and Information Sciences at Cambridge University Engineering Department and went on to complete his PhD in Information Engineering at the same institution. Following brief post-doctoral research positions at the Universities of Surrey and Cambridge, he was appointed Lecturer at the Department of Automatic Control & Systems Engineering at the University of Sheffield. He is currently Professor in Signal and Information Processing and is also the Director of the Rolls-Royce University Technology Centre for Control, Monitoring and Systems Engineering at Sheffield. His research interests are in the areas of modelling, signal processing and control with applications in aerospace, biomedical and other dynamic systems. He has published more than 200 papers in peer reviewed journals and conferences. His professional activities include being the Editor-in-Chief of the International Journal of Systems Science amongst other conference and journal activities.

Qing-Chang Zhong (M'04-SM'04-F'17) received two Ph.D. degrees, one from Imperial College London in 2004 and the other from Shanghai Jiao Tong University in 2000. He holds the Max McGraw Endowed Chair Professor in Energy and Power Engineering at Dept. of Electrical and Computer Engineering, Illinois Institute of Technology, and is the Founder & CEO of Syndem LLC, Chicago, USA. He serves/d as a Steering Committee member for IEEE Smart Grid, a Distinguished Lecturer for IEEE PELS/CSS/PES societies, an Associate Editor for IEEE TAC/TIE/TPELS/TCST/Access/JESTPE, and a Vice-Chair for IFAC TC Power and Energy Systems. He proposed the synchronized and democratized (SYNDEM) smart grid architecture to unify the integration of non-synchronous distributed energy resources and flexible loads. He is the (co-) author of four research monographs.

Alon Kuperman (M'07-SM'14) received the Ph.D. degree in Electrical and Computer Engineering from Ben-Gurion University of the Negev, Israel, in 2006 while being with Imperial College London as a Marie Curie Training Site Member. He was a Honorary Research Fellow with the University of Liverpool in 2008-2009. He is currently with the Department of Electrical and Computer Engineering, Ben-Gurion University, where he is heading the Power and Energy Systems track and the Applied Energy Laboratory. His research interests include all aspects of energy conversion and applied control.